Eur. Phys. J. C 41, 381–391 (2005)
Digital Object Identifier (DOI) 10.1140/epjc/s2005-02222-1

THE EUROPEAN PHYSICAL JOURNAL C

Probing new physics from top-charm associated productions at Linear Colliders

Junjie Cao[1,2], Guoli Liu[2], Jin Min Yang[2,3,a]

[1] Department of Physics, Henan Normal University, Henan 453002, P.R. China
[2] Institute of Theoretical Physics, Academia Sinica, Beijing 100080, P.R. China
[3] CCAST (World Laboratory), P.O. Box 8730, Beijing 100080, P.R. China

Received: 1 December 2004 / Revised version: 14 February 2005 /
Published online: 4 May 2005 –

Abstract. The top-charm associated productions via e^+e^-, $e^-\gamma$ and $\gamma\gamma$ collisions at linear colliders, which are extremely suppressed in the standard model (SM), could be significantly enhanced in some extensions of the SM. In this article we calculate the full contribution of the top-color-assisted technicolor (TC2) to these productions and then compare the results with the existing predictions of the SM, the general two-Higgs-doublet model and the minimal supersymmetric model. We find that the TC2 model predicts much larger production rates than other models and the largest-rate channel is $\gamma\gamma \to t\bar{c}$, which exceeds 10 fb for a large part of the parameter space. From the analysis of the observability of such productions at the future linear colliders, we find that the predictions of the TC2 model can reach the observable level for a large part of the parameter space while the predictions of other models are hardly accessible.

PACS. 4.65.Ha 12.60.Jv 11.30.Pb

1 Introduction

Since the measurements of top-quark properties in Run I at the Fermilab Tevatron have small statistics, there remains plenty of room for new physics in the top-quark sector. This stimulates a lot of efforts in the study of the top quark as a probe of new physics. Theoretical studies show that the top-quark processes are sensitive to new physics [1]. In some new physics models like the popular minimal supersymmetric model (MSSM) and the top-color-assisted technicolor (TC2) model [2–4], the top quark may have some exotic production and decay channels [5–18]. Among these exotic processes, one kind is induced by the flavor-changing neutral-current (FCNC) interactions, which are extremely suppressed in the SM but could be significantly enhanced in some extensions [7–18]. Searching for these exotic processes will serve as a good probe for new physics. Now such possibilities exist on our horizon: the ongoing Fermilab Tevatron collider, the upcoming CERN Large Hadron Collider (LHC) and the planned International Linear Collider (ILC) will allow one to scrutinize the top-quark nature [19].

Due to its rather clean environment, the ILC will be an ideal machine to probe new physics. In such a collider, in addition to e^+e^- collision, we can also realize $\gamma\gamma$ collisions and $e^-\gamma$ collisions with the photon beams generated by the backward Compton scattering of incident electron and laser beams [20]. The FCNC top-charm associated productions via e^+e^-, $e^-\gamma$ and $\gamma\gamma$ collisions will be a sensitive probe for different new physics models and should be seriously examined. While these processes have been studied thoroughly in the MSSM [13], the corresponding studies in the TC2 model are not complete: so far only the production at e^+e^- collision has been studied [16,17]. From the studies of these processes in the MSSM [13] we know that the e^+e^- collision channel has a much smaller rate than $\gamma\gamma$ collision or $e^-\gamma$ collision. So it is necessary to consider all the production channels to complete the calculations in TC2 models. This is one aim of this article.

The other aim of this article is to compare the $t\bar{c}$ production rates predicted by different new physics models. Such analysis will help to distinguish different models once the production rate is measured at the ILC.

The reason for examining the TC2 effects in such top-quark processes is two-fold. One is that the TC2 model is a popular realization of the fancy idea of technicolor and remains a typical candidate for new physics in the direction of dynamical symmetry breaking. This model has not been excluded by experiments so far and will face the test at future collider experiments. The other reason is that the TC2 model may have a richer top-quark phenomenology than other new physics models since it treats the top quark differently from other fermions. In fact, the TC2 model predicts some anomalous couplings for the top quark, among which the most notable ones occur in the flavor-changing sector [7]. So the TC2 model may predict

[a] e-mail: jmyang@itp.ac.cn

a large top-charm associated production rate and hence single it out from other new physics models.

This paper is organized as follows. Section 2 presents the calculations of the top-charm associated productions in TC2 model at the ILC. Section 3 compares the TC2 results with the predictions of the two-Higgs-doublet model and the MSSM. A discussion on observability at the ILC is given in Sect. 4 and the conclusion is given in Sect. 5.

2 Top-charm associated productions in the TC2 model

2.1 The relevant Lagrangian

Among various kinds of dynamical electroweak symmetry breaking models, the TC2 model [2–4] is especially attractive since it connects the top quark with the electroweak symmetry breaking (EWSB). In this model, the top-color interactions make small contributions to the EWSB, but give rise to the main part of the top-quark mass $(1-\epsilon)m_t$ with a model dependent parameter ϵ. The technicolor interactions play a main role in the EWSB, and the extended technicolor (ETC) interactions generate masses of lighter fermions and give a contribution ϵm_t to the full m_t. This model predicts some scalars such as top-pions $(\pi_t^0, \pi_t^\pm)$, which are condensates of the third-generation quarks and have strong couplings with the third-generation quarks. The existence of these new particles can be regarded as a typical feature of the TC2 model. Another feature of the TC2 model is the existence of large flavor-changing couplings [7,8]. In TC2 models the top-color interactions are non-universal and therefore do not posses a Glashow–Illiopoulos–Maiani (GIM) mechanism. These non-universal gauge interactions result in some FCNC vertices when one writes the interactions in the quark mass eigenbasis. Furthermore, the neutral scalars of the TC2 model as $t\bar{t}$ condensates also exhibit the same FCNC vertices. For instance, the interactions of top-pions take the form [2,7]

$$\begin{aligned}&\frac{m_t}{\sqrt{2}F_t}\frac{\sqrt{v_w^2-F_t^2}}{v_w}\\&\times\left[\mathrm{i}K_{UR}^{tt}K_{UL}^{tt*}\bar{t}_L t_R\pi_t^0+\sqrt{2}K_{UR}^{tt*}K_{DL}^{bb}\bar{t}_R b_L\pi_t^+\right.\\&\left.\quad+\mathrm{i}K_{UR}^{tc}K_{UL}^{tt*}\bar{t}_L c_R\pi_t^0+\sqrt{2}K_{UR}^{tc*}K_{DL}^{bb}\bar{c}_R b_L\pi_t^+ +\mathrm{h.c.}\right],\end{aligned}\tag{1}$$

where F_t is the top-pion decay constant, $v_w \equiv v/\sqrt{2} \simeq 174\,\mathrm{GeV}$, and K_{UL}, K_{DL} and K_{UR} are the rotation matrices that transform the weak eigenstates of left-handed up-type, down-type and right-handed up-type quarks to the mass eigenstates, respectively.

In the TC2 model, both the up-type and down-type quark mass matrices (M_U and M_D) exhibit an approximate triangle texture at the EWSB scale due to the generic top-color breaking pattern [2,21], which can severely restrict the forms of the matrices Ks in (1) and in turn, may lead to contradiction with the low energy data. Such a problem was addressed in [7] and it was observed that, given the textures of the mass matrices, it is possible to find a natural solution of the Ks to evade all the low energy constraints. In this solution, a realistic but simple pattern of K_{UL} and K_{DL} is constructed so that the measured CKM elements are reproduced, and further, the form of K_{UR}, the information of which is hidden in the SM, can be obtained using the expressions of M_U and K_{UL}. One distinctive character of K_{UR} is that the mixing between t_R and c_R can be naturally large, reaching 30%. This is what we are interested in. Values of the elements of the Ks relevant to our discussion are [7]

$$\begin{aligned}&K_{UL}^{tt}\simeq K_{DL}^{bb}\simeq 1,\quad K_{UR}^{tt}\simeq\frac{m_t'}{m_t}=1-\epsilon,\\&K_{UR}^{tc}\le\sqrt{1-K_{UR}^{tt\,2}}=\sqrt{2\epsilon-\epsilon^2},\end{aligned}\tag{2}$$

with m_t' denoting the top-color contribution to the top-quark mass. The TC2 model also predicts a CP-even scalar h_t, called top-Higgs [8], which is a $\bar{t}t$ bound state and analogous to the σ particle in low energy QCD. Its couplings to quarks are similar to that of the neutral top-pion except that the top-Higgs is CP-even while the neutral top-pion is CP-odd.

2.2 Analytical calculations

Since the TC2 contribution to the process $e^+e^- \to \gamma^*, Z^* \to t\bar{c}$ in e^+e^- collision has already been calculated in the literature [16,17], we focus on the processes $\gamma\gamma \to t\bar{c}$ in $\gamma\gamma$ collisions and $e^-\gamma \to e^-t\bar{c}$ in $e\gamma$ collisions. For completeness we will also take into account the process $e^+e^- \to e^+e^-\gamma^*\gamma^* \to e^+e^-t\bar{c}$ for e^+e^- collisions, where the γ^* particles are radiated out from the e^- and e^+ beams. Although it is a high-order process compared with $e^+e^- \to \gamma^*, Z^* \to t\bar{c}$, its contributions may not be underestimated since there is no s-channel suppression.

In the TC2 model, the process $\gamma\gamma \to t\bar{c}$ proceeds at loop level by exchanging the top-pions or top-Higgs. The corresponding Feynman diagrams are shown in Fig. 1. Compared with the corresponding diagrams in the MSSM [13], the contributions of TC2 model involve additional s-channel contributions, as shown in Fig. 1r. The effective coupling between top-pion (top-Higgs) and photons can be written as

$$\begin{aligned}\gamma\gamma\pi_t^0:\ &\frac{2\alpha_e Q_t^2}{\pi}\frac{m_t}{\sqrt{2}F_t}\frac{\sqrt{v_w^2-F_t^2}}{v_w}\frac{m_t}{s}\\&\times K_{UR}^{tt}K_{UL}^{tt*}c_1\left(\frac{s}{m_t^2}\right)\left(\mathrm{i}\epsilon_{\mu\nu\rho\lambda}k_1^\rho k_2^\lambda\right)\varepsilon_\mu(k_1,\lambda_1)\varepsilon_\nu(k_2,\lambda_2),\end{aligned}\tag{3}$$

$$\begin{aligned}\gamma\gamma h_t:\ &\frac{2\alpha_e Q_t^2}{\pi}\frac{m_t}{\sqrt{2}F_t}\frac{\sqrt{v_w^2-F_t^2}}{v_w}\frac{m_t}{s}\\&\times K_{UR}^{tt}K_{UL}^{tt*}c_2\left(\frac{s}{m_t^2}\right)\left(\frac{s}{2}g_{\mu\nu}-k_{1\nu}k_{2\mu}\right)\\&\quad\times\varepsilon_\mu(k_1,\lambda_1)\varepsilon_\nu(k_2,\lambda_2),\end{aligned}\tag{4}$$

where $s = 2k_1\cdot k_2$, $c_1(R) = \int_0^1 \mathrm{d}x \frac{\ln[1-Rx(1-x)]}{x}$, $c_2(R) = -2 + \left(1-\frac{4}{R}\right)c_1(R)$, Q_t is the electric charge of the top

quark, $k_{1,2}$ denote the momentum of the photons, and $\varepsilon_\nu(k_{1,2},\lambda_{1,2})$ are the polarization vectors of the photons. For the top-pion (top-Higgs) within the range between m_t and $2m_t$, the top-pion (top-Higgs) decays dominantly into $t\bar{c}$ [7,8][1] and thus such s-channel contributions become dominant if the CM energy of the $\gamma\gamma$ collision is high enough to produce a real top-pion (top-Higgs). In this case the cross section of top-charm associated production in the TC2 model may be quite large. In our calculation, we have considered all the decay channels of the top-pion and top-Higgs and have taken into account the width effects in the s-channel propagators.

Note that the reliability for doing such perturbative calculations should be carefully checked since the Yukawa couplings between the top-pion and the top quark might be large in the TC2 model. For example, from (1) we see that such a coupling strength is $Y = \frac{m_t}{\sqrt{2}F_t}\frac{\sqrt{v_w^2-F_t^2}}{v_w}$, which yields $Y^2/4\pi \simeq 0.44$ for a typical value of F_t ($F_t = 50\,\mathrm{GeV}$), a large value but still making the perturbative expansion valid. One may then wonder whether the perturbative expansion involving such large Yukawa couplings converge well, or, in other words, whether the TC2 Yukawa corrections to top-quark processes can drastically change the leading order predictions. Actually, such large Yukawa couplings are often present in new physics models such as the two-Higgs-doublet model [22] and the supersymmetric model [23] with small or large $\tan\beta$. One-loop Yukawa corrections to top production processes at hadron and linear colliders have been calculated [24], and it was observed that the corrections can maximally reach 30% in amplitude and drop rapidly as the scalars become heavy. So we believe that the perturbative expansion involving the TC2 Yukawa couplings is still a good expansion.

Another point that should be addressed is whether the top-pions can be regarded as point-like particles at the ILC energy. In the TC2 model the strong top-color gauge interaction causes the top-quark to condensate, which leads to the presence of top-pions. The compositeness scale of top-pions is about the mass scale of top-color gauge boson, which is usually assumed to be a few TeV [2,4]. So at the ILC energy (a few hundred GeV to 1 TeV), the top-pions can be regarded as point-like particles. Theoretically, the masses of top-pions can be quite light, well below the top-color scale, since they are a kind of pseudo-Goldstone bosons (a detailed discussion on their masses are given in the proceeding section) [2]. So the top-pions may be accessible at the ILC although the top-color scale is well above the ILC energy.

The magnitude of $\gamma\gamma \to t\bar{c}$ can be written as

$$\mathcal{M} = \frac{\alpha_e m_t^2}{4\pi F_t^2}\frac{v_w^2 - F_t^2}{v_w^2} \times K_{UR}^{tt*}K_{UR}^{tc}\sum_i \bar{u}_t\ \Gamma_i^{\mu\nu}\frac{1+\gamma_5}{2}\ v_c\varepsilon_\mu(k_1,\lambda_1)\varepsilon_\nu(k_2,\lambda_2), \tag{5}$$

where the sum is over all Feynman diagrams and for each diagram $F_i^{\mu\nu}$ takes the form

$$\begin{aligned}\Gamma_i^{\mu\nu} &= c_{i,1}p_t^\mu p_t^\nu + c_{i,2}p_c^\mu p_c^\nu + c_{i,3}p_t^\mu p_c^\nu + c_{i,4}p_t^\nu p_c^\mu \\ &+ c_{i,5}p_t^\mu\gamma^\nu + c_{i,6}p_c^\mu\gamma^\nu + c_{i,7}p_c^\nu\gamma^\mu + c_{i,8}p_t^\nu\gamma^\mu + c_{i,9}g^{\mu\nu} \\ &+ c_{i,10}\gamma^\nu\gamma^\mu + c_{i,11}p_t^\mu p_t^\nu \not{k}_2 + c_{i,12}p_c^\mu p_c^\nu \not{k}_2 + c_{i,13}p_t^\mu p_c^\nu \not{k}_2 \\ &+ c_{i,14}p_t^\nu p_c^\mu \not{k}_2 + c_{i,15}p_t^\mu\gamma^\nu \not{k}_2 + c_{i,16}p_c^\mu\gamma^\nu \not{k}_2 \\ &+ c_{i,17}p_c^\nu\gamma^\mu \not{k}_2 + c_{i,18}p_t^\nu\gamma^\mu \not{k}_2 + c_{i,19}g^{\mu\nu} \not{k}_2 \\ &+ c_{i,20}i\varepsilon^{\mu\nu\alpha\beta}\gamma_\alpha k_{2\beta} + c_{i,21}k_{1\mu}p_{t\nu} + c_{i,22}k_{1\mu}p_{c\nu} \\ &+ c_{i,23}k_{2\nu}p_{t\mu} + c_{i,24}k_{2\nu}p_{c\mu} + c_{i,25}k_{1\mu}\gamma_\nu + c_{i,26}k_{2\nu}\gamma_\mu \\ &+ c_{i,27}k_{1\mu}p_{t\nu} \not{k}_2 + c_{i,28}k_{1\mu}p_{c\nu} \not{k}_2 \\ &+ c_{i,29}k_{2\nu}p_{t\mu} \not{k}_2 + c_{i,30}k_{2\nu}p_{c\mu} \not{k}_2 + c_{i,31}k_{1\mu}\gamma_\nu \not{k}_2 \\ &+ c_{i,32}k_{2\nu}\gamma_\mu \not{k}_2. \end{aligned} \tag{6}$$

Here, $p_{t,c}$ are the momentum of outgoing top and charm quarks. The coefficients $c_{i,j}$ ($j = 1,\cdots,32$) can be obtained by a straightforward calculation of each Feynman diagram. For the sake of conciseness, we do not present their lengthy expressions here.

We checked that all ultraviolet divergences cancel out in our results, which is essentially guaranteed by the renormalizability. We also checked that our results satisfy the Ward identity, $k_1^\mu\Gamma_{\mu\nu} = 0$ and $k_2^\nu\Gamma_{\mu\nu} = 0$ with $\Gamma_{\mu\nu}$ being the sum of $\Gamma_{i\mu\nu}$. In fact, the s-channel contribution mediated by either top-pion or top-Higgs (shown in Fig. 1r) satisfies the Ward identity separately. This fact enables one to consider the s-channel contribution separately, as in [18]. For the convenience of our discussion, we will divide TC2 contributions into the s-channel contribution and the non-s-channel contribution, the latter of which includes the contributions from the t-channel, u-channel, quadric as well as box diagrams.

The $t\bar{c}$ production in $e^-\gamma$ collision proceeds through the process $e^-\gamma \to e^-\gamma^*\gamma \to e^-t\bar{c}$, where the γ beam is generated by the backward Compton scattering of incident electron and laser beam and the γ^* is radiated from e^- beam. The subprocess $\gamma^*\gamma \to t\bar{c}$ has the same Feynman diagrams as those shown in Fig. 1. In our calculation we use the Weizsäcker–Williams approximation [25] which treats γ^* from the e^- beam as a real photon. Thus the cross section is given by

$$\begin{aligned}&\hat{\sigma}_{e^-\gamma\to e^-t\bar{c}}(s_{e\gamma}) \\ &= \int_{(m_t+m_c)^2/s_{e\gamma}}^1 \mathrm{d}x\ P_{\gamma/e}(x,E_e)\ \hat{\sigma}_{\gamma\gamma\to t\bar{c}}(s_{\gamma\gamma} = xs_{e\gamma}),\end{aligned} \tag{7}$$

where $P_{\gamma/e}(x,E_e)$ is the probability of finding a photon with a fraction x of energy E_e in an ultra-relativistic electron and is given by [25]

$$\begin{aligned}&P_{\gamma/e}(x,E_e) \\ &= \frac{\alpha}{\pi}\left(\frac{1+(1-x)^2}{x}\left(\ln\frac{E_e}{m_e} - \frac{1}{2}\right)\right. \\ &\left. + \frac{x}{2}\left(\ln\left(\frac{2}{x}-2\right)+1\right) + \frac{(2-x)^2}{2x}\ln\left(\frac{2-2x}{2-x}\right)\right).\end{aligned} \tag{8}$$

[1] Depending on their masses, the decay products of neutral top-pion and top-Higgs may be $t\bar{t}$, $t\bar{c}$, $b\bar{b}$, gg,W^+W^-, Z^0Z^0,$\gamma\gamma$ and $Z^0\gamma$. Generally speaking, the dominant decay mode is $t\bar{t}$ for $m_{\pi_t,h_t} > 2m_t$, $t\bar{c}$ for $m_t < m_{\pi_t,h_t} < 2m_t$ and $b\bar{b}$ for $m_{\pi_t,h_t} < m_t$.

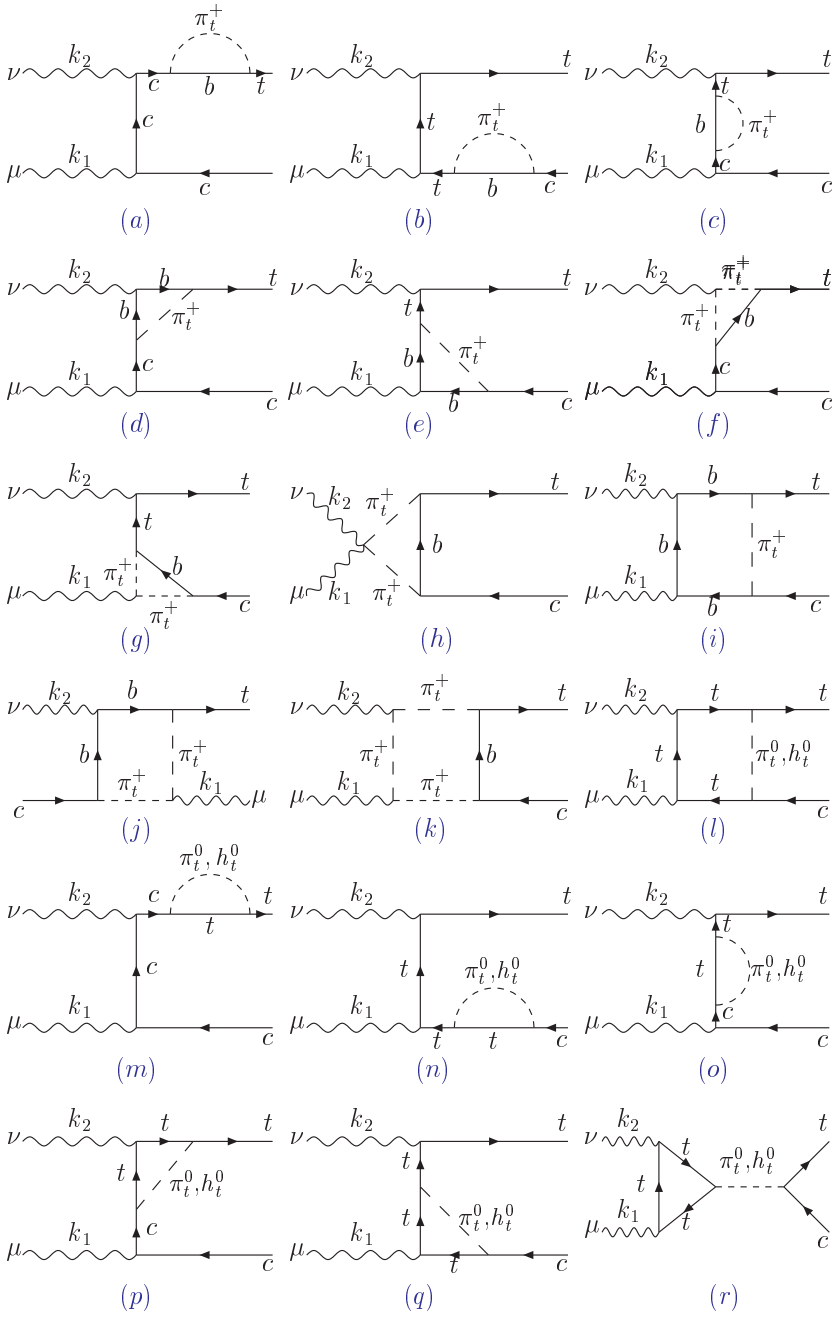

Fig. 1. Feynman diagrams contributing to the process $\gamma\gamma \to t\bar{c}$ in the TC2 model. Those obtained by exchanging the two external photon lines are not displayed here

Note that the incoming electron may also radiate a Z-boson to contribute to the process $e^-\gamma \to e^- t\bar{c}$. However, such a contribution is suppressed by the probability function of finding a Z-boson in an ultra-relativistic electron [26] and can be safely neglected.

As for $e^+e^- \to e^+e^-\gamma^*\gamma^* \to e^+e^-t\bar{c}$ in e^+e^- collisions, its cross section can be obtained by folding $P_{\gamma/e}$ with $\hat{\sigma}_{\gamma\gamma\to t\bar{c}}$, as done in (7),

$$\begin{aligned}
&\sigma_{e^+e^-\overset{\gamma^*\gamma^*}{\to} e^+e^-t\bar{c}}(s_{e^+e^-}) \\
&= \int_a^1 \mathrm{d}x \int_{a/x}^1 \mathrm{d}y P_{\gamma/e}(x, E_{e^+}) P_{\gamma/e}(y, E_{e^-}) \\
&\quad \times \hat{\sigma}_{\gamma\gamma\to t\bar{c}}(s_{\gamma\gamma} = xys_{e^+e^-}) \\
&= \int_{\sqrt{a}}^1 2z\mathrm{d}z\ \hat{\sigma}_{\gamma\gamma\to t\bar{c}}(s_{\gamma\gamma} = z^2 s_{e^+e^-}) \\
&\quad \times \int_{z^2}^1 \frac{\mathrm{d}x}{x}\ P_{\gamma/e}(x, E_{e^+}) P_{\gamma/e}\left(\frac{z^2}{x}, E_{e^-}\right), \qquad (9)
\end{aligned}$$

where we define $a = (m_t + m_c)^2/s_{e^+e^-}$. In the TC2 model, it is argued that the top-Higgs may couple directly with ZZ or W^+W^- [7]. If so, the processes $e^+e^- \to e^+e^-ZZ \to e^+e^-t\bar{c}$ and $e^+e^- \to \nu\bar{\nu}W^+W^- \to \nu\bar{\nu}t\bar{c}$ may also be important for top-charm associated production at e^+e^- collision [17]. We will take the results of [17] for comparison in our discussions.

For both $\gamma\gamma$ collision and $e\gamma$ collisions, the photon beams are generated by the backward Compton scattering of incident electron and laser beams just before the interaction point. The event number is obtained by convoluting the cross section with the photon beam luminosity distribution. For a $\gamma\gamma$ collider the event number is obtained by

$$N_{\gamma\gamma\to t\bar{c}} = \int \mathrm{d}\sqrt{s_{\gamma\gamma}} \frac{\mathrm{d}\mathcal{L}_{\gamma\gamma}}{\mathrm{d}\sqrt{s_{\gamma\gamma}}} \hat{\sigma}_{\gamma\gamma\to t\bar{c}}(s_{\gamma\gamma}) \equiv \mathcal{L}_{e^+e^-}\ \sigma_{\gamma\gamma\to t\bar{c}}(s_{e^+e^-}), \quad (10)$$

where $\mathrm{d}\mathcal{L}_{\gamma\gamma}/\mathrm{d}\sqrt{s_{\gamma\gamma}}$ is the photon beam luminosity distribution and $\sigma_{\gamma\gamma\to t\bar{c}}(s_{e^+e^-})$, with $s_{e^+e^-}$ being the energy-square of e^+e^- collision, is defined as the effective cross section of $\gamma\gamma \to t\bar{c}$. In the optimum case, it can be written as [27]

$$\sigma_{\gamma\gamma\to t\bar{c}}(s_{e^+e^-}) = \int_{\sqrt{a}}^{x_{\max}} 2z\mathrm{d}z\ \hat{\sigma}_{\gamma\gamma\to t\bar{c}}(s_{\gamma\gamma} = z^2 s_{e^+e^-}) \times \int_{z^2/x_{\max}}^{x_{\max}} \frac{\mathrm{d}x}{x}\ F_{\gamma/e}(x)\ F_{\gamma/e}\left(\frac{z^2}{x}\right), \quad (11)$$

where $F_{\gamma/e}$ denotes the energy spectrum of the back-scattered photon for an unpolarized initial electron and laser photon beams given by

$$F_{\gamma/e}(x) = \frac{1}{D(\xi)}\left(1 - x + \frac{1}{1-x} - \frac{4x}{\xi(1-x)} + \frac{4x^2}{\xi^2(1-x)^2}\right). \quad (12)$$

The definitions of the parameters ξ, $D(\xi)$ and $x_{\max}$ can be found in [27]. In our numerical calculation, we choose $\xi = 4.8$, $D(\xi) = 1.83$ and $x_{\max} = 0.83$.

For the $e^-\gamma$ collider the effective cross section of $e\gamma \to et\bar{c}$ is defined as

$$\sigma_{e^-\gamma\to e^-t\bar{c}}(s_{e^+e^-}) = \frac{1}{\mathcal{L}_{e^+e^-}} \int \mathrm{d}\sqrt{s_{e\gamma}} \frac{\mathrm{d}\mathcal{L}_{e\gamma}}{\mathrm{d}\sqrt{s_{e\gamma}}}\ \hat{\sigma}_{e^-\gamma\to e^-t\bar{c}}(s_{e\gamma}) = \int_{\sqrt{a}}^{\sqrt{x_{\max}}} 2z\mathrm{d}z\ \hat{\sigma}_{\gamma\gamma\to t\bar{c}}(s_{\gamma\gamma} = z^2 s_{e^+e^-}) \times \int_{z^2/x_{\max}}^{1} \frac{\mathrm{d}x}{x}\ P_{\gamma/e}(x, E_e) F_{\gamma/e}\left(\frac{z^2}{x}\right). \quad (13)$$

From above analysis, especially from (9), (11) and (13), we know that the cross sections for $e^+e^- \overset{\gamma^*\gamma^*}{\to} e^+e^-t\bar{c}$, $e^-\gamma \to e^-t\bar{c}$ and $\gamma\gamma \to t\bar{c}$ are connected by convoluting the same $\hat{\sigma}_{\gamma\gamma\to t\bar{c}}$ with different photon distribution functions. Noting the fact that $F_{\gamma/e} > P_{\gamma/e}$ for the integrated range of x, one can infer that the cross section at $\gamma\gamma$ collider is the largest, which will be shown in our results. In the following the major part of discussions will be focused on the production in $\gamma\gamma$ collisions.

2.3 Numerical results

In our numerical study, the bottom and charm quark masses will be neglected, and the charge conjugate $\bar{t}c$ production channel is also included. The cross sections of top-charm associated productions in the TC2 model depend on ϵ, K_{UR}^{tc}, the top-pion decay constant F_t and the masses of the top-pions and top-Higgs. Before starting numerical calculations, we recapitulate the theoretical and experimental constraints on these parameters.

(1) About the ϵ parameter: in the TC2 model, ϵ parameterizes the portion of ETC contribution to the top-quark mass. The bare value of ϵ is generated at the ETC scale, and subject to very large radiative enhancement from top-color and $U(1)_{Y_1}$ by a factor of order 10 when evolving down to the weak scale [2]. This ϵ can induce a non-zero top-pion mass (proportional to $\sqrt{\epsilon}$) [28] and thus ameliorate the problem of having dangerously light scalars. Numerical analysis shows that, with a reasonable choice of the other input parameters, ϵ of order $10^{-2} \sim 10^{-1}$ may induce top-pions as to be massive as the top quark [2]. Indirect phenomenological constraints on ϵ come from low energy flavor-changing processes such as $b \to s\gamma$ [29]. However, these constraints are very weak. A precise value of ϵ may be obtained by elaborately measuring the coupling strength between top-pion/top-Higgs and tops at the linear colliders. From the theoretical point of view, an ϵ with value from 0.01 to 0.1 is favored. For the considered process in our analysis, the non-zero ϵ contributes a factor of $(1-\epsilon)^2$ (through $(K_{UR}^{tt})^2$) to the cross section (see (5)), and thus the results are not sensitive to ϵ in the range of $0.01 \sim 0.1$. Throughout this paper, we fix conservatively $\epsilon = 0.1$.

(2) The parameter K_{UR}^{tc} is upper bounded by the unitary relation $K_{UR}^{tc} \leq \sqrt{1 - K_{UR}^{tt\,2}} = \sqrt{2\epsilon - \epsilon^2}$. For an ϵ value smaller than 0.1, this corresponds to $K_{UR}^{tc} < 0.43$. In our analysis, we will treat K_{UR}^{tc} as a free parameter.

(3) About the top-pion decay constant F_t: the Pagels–Stokar formula [30] gives an expression for it in terms of the number of quark color N_c, the top-quark mass, and the scale Λ at which the condensation occurs:

$$F_t^2 = \frac{N_c}{16\pi^2} m_t^2 \ln\frac{\Lambda^2}{m_t^2}. \quad (14)$$

From this formula, one can infer that, if $t\bar{t}$ condensation is fully responsible for EWSB, i.e. $F_t \simeq v_w \equiv v/\sqrt{2} = 174\,\mathrm{GeV}$, then Λ is about $10^{13} \sim 10^{14}\,\mathrm{GeV}$. Such a large value is less attractive since by the original idea of technicolor theory [31], one expects that the new physics scale should not be far higher than the weak scale. On the other hand, if one believes new physics exists at the TeV scale, i.e. $\Lambda \sim 1\,\mathrm{TeV}$, then $F_t \sim 50\,\mathrm{GeV}$, which means that $t\bar{t}$ condensation alone cannot be wholly responsible for EWSB and to break electroweak symmetry needs the joint effort of top-color and other interactions like technicolor. From the experimental point of view, probably the best way to determine F_t is by precisely measuring the coupling strength of the top-Higgs with vector bosons at future linear collider, which is proportional to F_t without

any theoretical ambiguity [8]. By the way, (14) should be understood as only a rough guide, and F_t may in fact be somewhat lower or higher, say in the range $40 \sim 80\,\mathrm{GeV}$. Allowing F_t to vary over this range does not qualitatively change our conclusion, and, therefore, we use the value $F_t = 50\,\mathrm{GeV}$ for illustration in our numerical analysis.
(4) About the mass bounds for top-pions and top-Higgs: on the theoretical side, some estimates have been done. The mass splitting between the neutral top-pion and the charged top-pion should be small since it comes only from the electroweak interactions [32]. Reference [2] has estimated the mass of top-pions using the quark loop approximation and showed that m_{π_t} is allowed to be a few hundred GeV in a reasonable parameter space. Like (14), such estimations can only be regarded as a rough guide and the precise values of top-pion masses can be determined only by future experiments. The mass of the top-Higgs h_t can be estimated in the Nambu–Jona–Lasinio (NJL) model in the large N_c approximation and is found to be about $2m_t$ [8]. This estimation is also rather crude and the mass below the $\bar{t}t$ threshold is quite possible in a variety of scenarios [33]. On the experimental side, current experiments have restricted the mass of the charged top-pion. For example, the absence of $t \to \pi_t^+ b$ implies that $m_{\pi_t^+} > 165\,\mathrm{GeV}$ [34] and R_b analysis yields $m_{\pi_t^+} > 220\,\mathrm{GeV}$ [35,36]. For the neutral top-pion and top-Higgs, the experimental restrictions on them are rather weak. (Of course, considering theoretically that the mass splitting between the neutral and charged top-pions is small, the R_b bound on the charged top-pion mass should be applicable to the neutral top-pion masses.) The current bound on techni-pions [37] does not apply here since the properties of top-pion are quite different from those of techni-pions. The direct search for the neutral top-pion (top-Higgs) via $pp \to t\bar{t}\pi_t^0(h_t)$ with $\pi_t^0(h_t) \to b\bar{b}$ was proven to be hopeless at Tevatron for the top-pion (top-Higgs) heavier than 135 GeV [38]. The single production of π_t^0 (h_t) at Tevatron with π_t^0 (h_t) mainly decaying to $t\bar{c}$ may shed some light on detecting the top-pion (top-Higgs) [8], but the potential for the detection is limited by the value of K_{UR}^{tc} and the detailed background analysis is absent now. Anyhow, these mass bounds will be greatly tightened at the upcoming LHC [7,9,38]. Combining the above theoretical and experimental bounds, we will assume

$$m_{\pi_t^0} = m_{\pi_t^+} \equiv m_{\pi_t} > 220\,\mathrm{GeV}. \tag{15}$$

Figure 2 shows the dependence of the cross section of $\gamma\gamma \to t\bar{c}$ on m_{π_t} under the assumption $m_{\pi_t} = m_{h_t}$. One sees that for $m_{\pi_t} > 220\,\mathrm{GeV}$, the cross section first increases monotonously to reach its maximum value at $m_{\pi_t} = 2m_t$, and then drops rapidly. This behavior may be explained as follows. For the results in Fig. 2, the dominant contributions are from the s-channel diagrams (we will comment on the effects of the non-s-channel diagrams later), and the cross section then may be estimated by the narrow width approximation (note that there is no interference between the contribution from the top-pion and that from the top-Higgs due to the different CP property

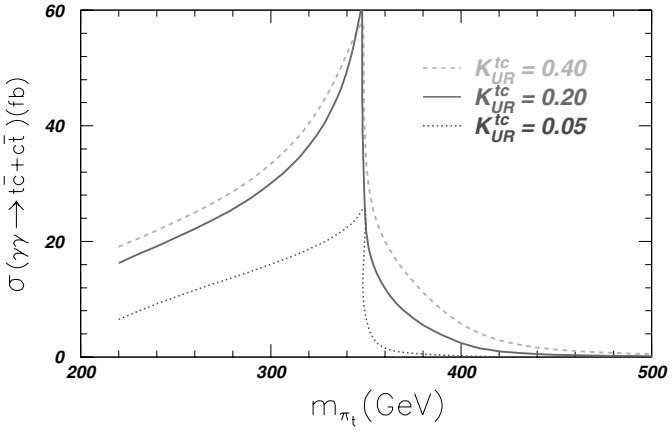

Fig. 2. The m_{π_t} dependence of the cross section in $\gamma\gamma$ collision for $\sqrt{s_{e^+e^-}} = 500\,\mathrm{GeV}$ under the assumption $m_{\pi_t} = m_{h_t}$

of π_t^0 and h_t):

$$\begin{aligned}&\sigma(\gamma\gamma \to t\bar{c})\\ &= \sigma(\gamma\gamma \to \pi_t^0)\mathrm{Br}(\pi_t^0 \to t\bar{c})\\ &\quad +\sigma(\gamma\gamma \to h_t)\mathrm{Br}(h_t \to t\bar{c}),\end{aligned} \tag{16}$$

where $\sigma(\gamma\gamma \to \pi_t^0(h_t))$ is the rate for single top-pion (top-Higgs) production, and $\mathrm{Br}(\pi_t^0(h_t) \to t\bar{c})$ is the branching fraction for $\pi_t^0(h_t) \to t\bar{c}$. In the range $m_t + m_c < m_{\pi_t} < 2m_t$, the cross section increases with m_{π_t} since the $t\bar{c}$ decay mode of $\pi_t^0(h_t)$ is getting a larger branching ratio and becoming dominant as m_{π_t} increases. When m_{π_t} passes the threshold of $2m_t$ and keeps increasing, the cross section drops quickly since the $t\bar{t}$ is becoming the dominant decay mode of $\pi_t^0(h_t)$, and $\sigma(\gamma\gamma \to \pi_t^0(h_t))$ is getting severely suppressed by the photon luminosity distribution.

Figure 2 shows that the $t\bar{c}$ production rate in $\gamma\gamma$ collision can exceed 10 fb. Comparing with $e^+e^- \to t\bar{c}$ in e^+e^- collision, which can only reach 0.1 fb in the TC2 model [16] due to the s-channel suppression, one may infer that the $\gamma\gamma$ collision may be much better in probing the TC2 model. We will elaborate the observability of the top-charm associated production at the ILC in Sect. refsec4. Since we only intend to figure out the typical order of the production rate for such rare processes, we fix $K_{UR}^{tc} = 0.4$ for illustration in our following analysis.

Now we comment on the effects of the non-s-channel diagrams in Fig. 1. There are two features for such effects. One is that they are proportional to K_{UR}^{tc}, and, therefore, may be sizable only for large values of K_{UR}^{tc}. The other is that they generally increase with the enhancement of the CM energy of the collider. For $K_{UR}^{tc} = 0.4$, $\sqrt{s_{e^+e^-}} = 500\,\mathrm{GeV}$ and $m_{\pi_t} = m_{h_t}$, our findings are as follows.
(a) In the most interesting range, $m_t < m_{\pi_t} < 2m_t$, the cross section is dominated by the s-channel contributions. The non-s-channel effects, which in this case arise mainly from the interference with the s-channel diagrams, are less than 3%. The main reason is that, as pointed out earlier, in this region $t\bar{c}$ is the dominant decay mode of π_t^0 and h_t produced in the s-channel. Another reason is that un-

der our assumption $m_{\pi_t} = m_{h_t}$ there exists a cancellation between the top-pion non-s-channel diagrams and the top-Higgs non-s-channel diagrams.
(b) In the heavy range, $m_{\pi_t} > 2m_t$, which is less interesting since the cross section is too small (as shown in Fig. 2), the cross section is also dominated by the s-channel contributions due to the cancellation of the non-s-channel top-pion and top-Higgs diagrams mentioned above.
(c) In the light range, $m_{\pi_t} < m_t$, which is disfavored by R_b [35,36], and thus the corresponding results are not shown here; the non-s-channel contributions are dominant. In this region the s-channel contributions are suppressed since the top-pions and the top-Higgs in the s-channel cannot be on-shell. The non-s-channel contributions are quite large in this region due to the following two reasons. One is that $u - m_c^2$ (for the u-channel) and $t - m_c^2$ (for the t-channel) in the propagators of the charm quark (see Fig. 1a,c,d,f,m,p) can approach zero[2] and thus the non-s-channel contributions can be greatly enhanced. In fact, this is the advantage of a $\gamma\gamma$ collider over an e^+e^- collider in exploring the top-quark FCNC processes, as pointed out in [39]. The other reason is that the contributions from the box diagrams of Fig. 1i–k are also quite sizable for light top-pions. From our numerical evaluation we found that in the region $m_{\pi_t} < m_t$, among the non-s-channel diagrams, the charged top-pion diagrams give dominant contributions and the cross section peaks at $m_{\pi_t} \simeq 140\,\mathrm{GeV}$ with $\sigma_{\max} \simeq 25\,\mathrm{fb}$.
(d) Note that our above analyses are under the assumption $m_{h_t} = m_{\pi_t}$. Although there is a good reason [32] to expect the mass degeneracy for neutral and charged top-pions, the top-Higgs mass m_{h_t} may be quite different from the top-pion mass $m_{\pi_t}(= m_{\pi_t^0} = m_{\pi_t^+})$. If we allow for a splitting between m_{h_t} and m_{π_t}, we found that in the allowed range of m_{π_t} (i.e. $> 220\,\mathrm{GeV}$), the non-s-channel contributions can be as large as 16% for a relatively light top-Higgs, as shown in Fig. 3.

So we conclude to the following.
(i) Under the assumption $m_{\pi_t} = m_{h_t}$, the cross section is dominated by the s-channel contributions and the non-s-channel effects are negligibly small for $m_{\pi_t} > m_t$. Only in the case of $m_{\pi_t} < m_t$, which is disfavored by the R_b bound, the non-s-channel contributions can be quite large and dominant.
(ii) Without the assumption $m_{\pi_t} = m_{h_t}$, for a relatively light top-Higgs, the non-s-channel contributions can be as large as 16% for the allowed range of m_{π_t} (i.e. $> 220\,\mathrm{GeV}$).

In Fig. 4 we plot the contours of the cross section in the plane of K_{UR}^{tc} versus m_{π_t} under the assumption $m_{h_t} = m_{\pi_t}$. One can learn that as long as m_{π_t} is lower than 400 GeV, there exists a large parameter space where the cross section can exceed 2 fb. Especially for $m_{\pi_t} \simeq 2m_t$, the parameter K_{UR}^{tc} can be explored to values as small as 10^{-2} given that the production rate $\sigma \simeq 2\,\mathrm{fb}$ is accessible at the ILC.

[2] Setting $m_c = 0$ does not develop poles for the cross section since the poles from the u-channels are canceled by those from the t-channels.

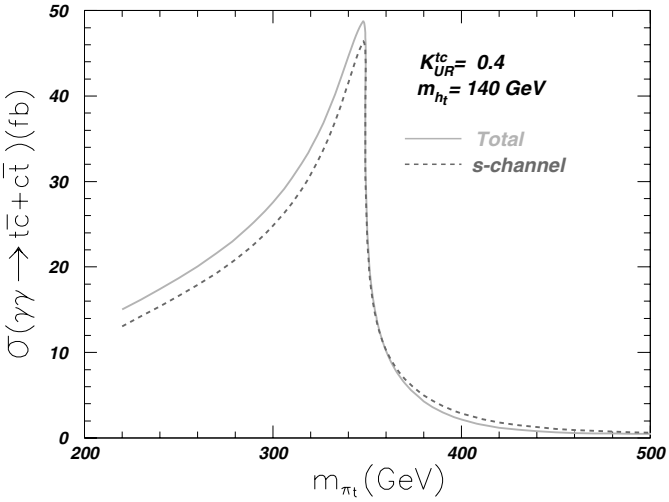

Fig. 3. The m_{π_t} dependence of the cross section of $\gamma\gamma \to t\bar{c}$ for $\sqrt{s_{e^+e^-}} = 500\,\mathrm{GeV}$. The solid curve is the total contribution from both s-channel and non-s-channel diagrams, while the dashed one is the contribution from only the s-channel diagrams

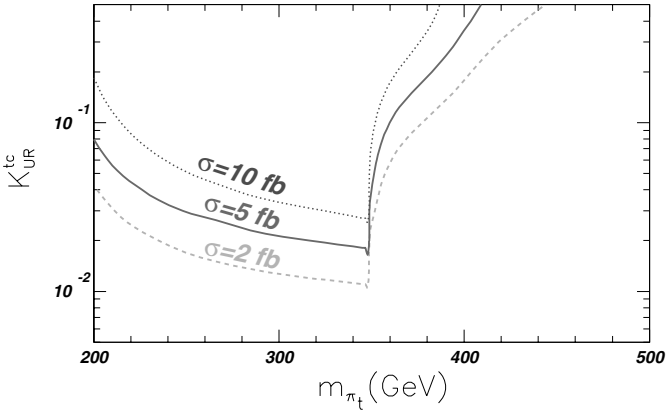

Fig. 4. Contours of the cross section of $\gamma\gamma \to t\bar{c}$ in the plane of K_{UR}^{tc} versus m_{π_t} for $\sqrt{s_{e^+e^-}} = 500\,\mathrm{GeV}$

In Fig. 5, we show the behavior of the rates for $\gamma\gamma \to t\bar{c}$, $e^-\gamma \to e^-t\bar{c}$ and $e^+e^- \overset{\gamma^*\gamma^*}{\to} e^+e^-t\bar{c}$ versus the collider energy. As illustrated in the figure, the $\sigma(\gamma\gamma \to t\bar{c})$ is insensitive to the collider energy for $E_{cm} > 400\,\mathrm{GeV}$ while the other two channels rise significantly with the collider energy, which can be explained by the energy dependence of $P_{\gamma/e}$.

Figure 5 shows that $\sigma(\gamma\gamma \to t\bar{c}) \gg \sigma(e^-\gamma \to e^-t\bar{c}) \gg \sigma(e^+e^- \overset{\gamma^*\gamma^*}{\to} e^+e^-t\bar{c})$. Since the s-channel process $e^+e^- \to \gamma^*, Z^* \to t\bar{c}$ is suppressed by the propagators of the intermediate photon or Z-boson and was found [16] to occur at a similar rate as $e^+e^- \overset{\gamma^*\gamma^*}{\to} e^+e^-t\bar{c}$ shown in Fig. 5, we conclude that the production rate in $\gamma\gamma$ collisions is largest at a linear collider.

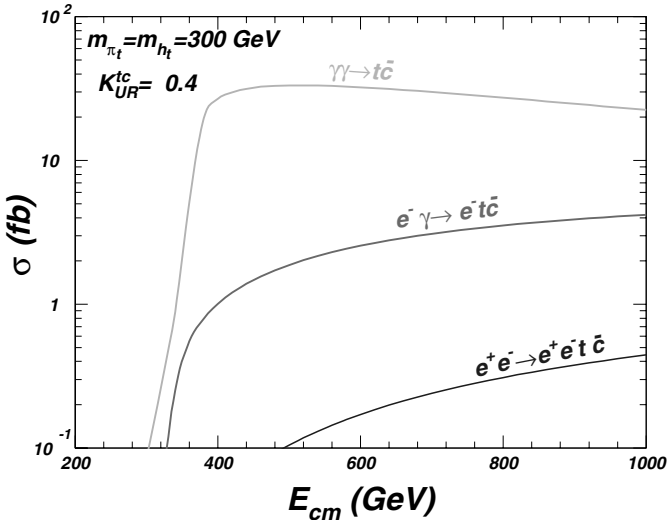

Fig. 5. The cross sections versus the e^+e^- center-of-mass energy

3 Comparison of the predictions of different models

In this section, we first briefly recapitulate the sources of FCNC transitions in different models and then compare the typical magnitudes of various FCNC processes at the ILC predicted by different models. We arrive at the observation that the TC2 model predicts much larger FCNC transitions than other new physics models.

It is well known that in the SM the FCNC transitions are absent at tree level and can occur only at loop level by the GIM mechanism. The source of such FCNC transitions is the non-diagonality of the Cabbibo–Kobayashi–Maskawa (CKM) matrix. In the extensions of the SM, although the CKM matrix can still induce additional contributions to FCNC via loops composed by new particles, some new sources for FCNC transitions usually come in.

As the simplest extension of the SM, the two-Higgs-doublet model (2HDM) may naturally have an FCNC mediated by the Higgs bosons at tree level, unless some ad hoc discrete symmetry is imposed. The generic type of 2HDM is the so-called "type-III" model (2HDM-III) [22, 40], in which the up-type and down-type quarks couple to both Higgs doublets and thus the diagonalization of the quark mass matrices does not automatically ensure the diagonalization of the Yukawa couplings. In a popular realization of 2HDM-III, one Higgs doublet is responsible for the electroweak symmetry breaking as well as generating the fermion masses while the other doublet has FCNC couplings whose strength are usually parameterized as [22]

$$\xi^{U,D}_{ij} = \lambda^{U,D}_{ij}\frac{\sqrt{m_i m_j}}{v}, \tag{17}$$

with $i,j = 1,2,3$ being the generation indices, m_i the quark masses and λ_{ij} the dimensionless parameters. From (17), we can learn that the FCNC coupling without top quark is generally suppressed by the involved quark masses. One impressive feature of 2HDM-III is that the coupling strengths of the FCNC are related with those of flavor-changing charged currents. The FCNC couplings λ^U_{tc} and λ^U_{ct} then contribute to some low energy observable and the bounds from low energy data are λ^U_{tc}, $\lambda^U_{ct} \sim O(1)$ [40].

The MSSM [23] also contains two Higgs doublets. However, the homology of the superpotential requires that one doublet couples only to up-type quarks while the other doublet couples only to down-type quarks and hence avoids tree-level FCNC transitions in the Higgs sector. Note that when supersymmetry is broken, the couplings QUH_d and QDH_u are generated at one-loop level to induce FCNC Yukawa couplings. While such FCNC couplings are generally small for up-type quarks, they may be quite large for down-type quarks due to the enhancement by large $\tan\beta$ [41]. Another source of FCNC in the MSSM is the flavor mixings of sfermions [23,42], which induce FCNC transitions in the fermion sector through loops composed by sparticles, such as the sfermion–gaugino loop and the sfermion–Higgsino loop [12].

As discussed in Sect. 2, the TC2 model, as one of the dynamic EWSB models, is quite different from the 2HDM and the MSSM. In this model, the scalar bosons are composite particles with properties quite similar to those of Higgs bosons. One distinguished character of the TC2 model is that the third-generation quarks are special and have a new top-color interaction [2]. This non-universal top-color interaction can result in FCNC transitions when expressing the interactions in terms of quark mass eigenstates. In particular, the triangle texture of the up-type quark mass matrix due to the generic top-color breaking pattern can lead to large flavor mixing between t_R and c_R [7,8]. Furthermore, the FCNC transitions also exhibit themselves in the neutral scalar sector, which are $t\bar{t}$ condensates. Therefore, the top flavor phenomenology is much richer in this model than in other models.

So far as the top-charm associated productions are concerned, in the SM they are severely suppressed since they proceed through loops comprising of light down-type quarks (much lighter than the top-quark mass scale) and involving the small mixings between the third-generation quarks and the quarks of the first two generations. Table 1 shows the rates for $e^+e^- \to t\bar{c}$, $e\gamma \to et\bar{c}$ and $\gamma\gamma \to t\bar{c}$ at the ILC. As can be seen, the rates predicted by the SM are too small to be accessible at the ILC.

In 2HDM-III, the process $\gamma\gamma \to t\bar{c}$ proceeds in a way similar to that in the TC2 model except that the top-pions and top-Higgs in Fig. 1 should be replaced by the corresponding Higgs bosons. However, due to the smallness of λ^U_{tc}, its cross section is generally two orders lower than in the TC2 model. In Table 1, we present the predictions of 2HDM-III for various production channels at the ILC. One impressive feature is that the rates of $e^+e^- \overset{Z^*Z^*}{\to} e^+e^-t\bar{c}$ and $e^+e^- \overset{W^*W^*}{\to} \nu\bar{\nu}t\bar{c}$ is comparable to $\gamma\gamma \to t\bar{c}$ and much larger than $e^+e^- \to t\bar{c}$. The reason is that in 2HDM-III the Higgs bosons may couple at tree level with ZZ or W^+W^- and, consequently, despite the suppression of the

Table 1. Theoretical predictions for top-quark FCNC processes. The predictions of new physics models are optimum values. The e^+e^- collider energy is 500 GeV for production processes. The cross sections are in the units of fb. The processes not referenced are estimated by us

	SM	2HDM-III	MSSM	TC2
$\sigma(\gamma\gamma \to t\bar{c})$	$\mathcal{O}(10^{-8})$ [13]	$\mathcal{O}(10^{-1})$ [15]	$\mathcal{O}(10^{-1})$ [13]	$\mathcal{O}(10)$
$\sigma(e\gamma \to et\bar{c})$	$\mathcal{O}(10^{-9})$ [13]	$\mathcal{O}(10^{-2})$	$\mathcal{O}(10^{-2})$ [13]	$\mathcal{O}(1)$
$\sigma(e^+e^- \to t\bar{c})$	$\mathcal{O}(10^{-10})$ [44,13]	$\mathcal{O}(10^{-3})$ [45]	$\mathcal{O}(10^{-2})$ [13]	$\mathcal{O}(10^{-1})$ [16]
$\sigma(e^+e^- \overset{\gamma^*\gamma^*}{\to} e^+e^-t\bar{c})$	$< 10^{-10}$ [13]	$\mathcal{O}(10^{-3})$	$\mathcal{O}(10^{-3})$ [13]	$\mathcal{O}(10^{-1})$
$\sigma(e^+e^- \overset{Z^*Z^*}{\to} e^+e^-t\bar{c})$	$< 10^{-10}$	$\mathcal{O}(10^{-1})$ [43]	$< 10^{-3}$	$\mathcal{O}(1)$ [17]
$\sigma(e^+e^- \overset{\gamma^*Z^*}{\to} e^+e^-t\bar{c})$	$< 10^{-10}$	$< 10^{-3}$	$< 10^{-3}$	$< 10^{-1}$
$\sigma(e^+e^- \overset{W^*W^*}{\to} \nu\bar{\nu}t\bar{c})$	$< 10^{-10}$	$\mathcal{O}(10^{-1})$ [43]	$< 10^{-3}$	$\mathcal{O}(1)$ [17]
$\mathrm{Br}(t \to cg)$	$\mathcal{O}(10^{-11})$ [46]	$\mathcal{O}(10^{-5})$ [47]	$\mathcal{O}(10^{-5})$ [12,13]	$\mathcal{O}(10^{-4})$ [11]
$\mathrm{Br}(t \to cZ)$	$\mathcal{O}(10^{-13})$ [46]	$\mathcal{O}(10^{-6})$ [47]	$\mathcal{O}(10^{-7})$ [12,13]	$\mathcal{O}(10^{-4})$ [11]
$\mathrm{Br}(t \to c\gamma)$	$\mathcal{O}(10^{-13})$ [46]	$\mathcal{O}(10^{-7})$ [47]	$\mathcal{O}(10^{-7})$ [12,13]	$\mathcal{O}(10^{-6})$ [11]
$\mathrm{Br}(t \to ch)$	$< 10^{-13}$ [46]	$\mathcal{O}(10^{-3})$	$\mathcal{O}(10^{-4})$ [48]	$\mathcal{O}(10^{-1})$

probability to find the gauge bosons in an electron, its cross section may still be large [43].

In the MSSM, $\gamma\gamma \to t\bar{c}$ proceeds via the loops comprising squarks, gluinos, charginos and neutralinos. The corresponding results in Table 1 are taken from [13] where only SUSY-QCD contributions are considered[3]. As shown in Table 1, the cross sections in the MSSM, although they can be much larger than the SM predictions, are generally much smaller than the TC2 predictions. The reason is two-fold. One reason is that in the MSSM there is no s-channel contribution like that shown in Fig. 1r at one-loop level. The other reason is that there are cancellations between different diagrams due to the unitarity of the matrix diagonalizing the up-type squark mass matrix, which is often called the "super-GIM" mechanism.

For completeness we also present the branching ratios of various rare top decays in Table 1. It may be surprising that the branching ratio of $t \to ch_t$ can reach 10^{-1} in the TC2 model if the top-Higgs is light. In fact, this does not contradict current experiments due to the small statistics of current top-quark measurements [19,49]. A future bound on $t \to ch_t$ will not influence the optimum magnitude of $\gamma\gamma \to t\bar{c}$ since the favored region for the latter process is $m_{h_t} = 200 \sim 300\,\mathrm{GeV}$.

We conclude from Table 1 that the TC2 model generally predicts much larger top-quark FCNC transitions than any other models and the $\gamma\gamma$ collision is the best channel in enhancing the magnitude for the top-charm associated productions at the ILC.

[3] To our knowledge, the SUSY electroweak contributions to top-charm associated production have not yet been calculated. However, from the fact that the SUSY-QCD contributions to the rare decay $t \to c\gamma$ is generally larger than SUSY electroweak contributions [12], we may infer that the SUSY-QCD contributions represent the typical size of SUSY contributions.

4 Observability of top-charm production at ILC

Given the predictions listed in Table 1, we now discuss their observability at the ILC. First, for the top rare decays other than $t \to ch$, the hope to observe them at the ILC is dim since only about 10^4 top-quark events can be produced for an integrated luminosity of $100\,\mathrm{fb}^{-1}$ at the ILC [19,50]. For the top-charm associated production processes, the observability is analyzed in the following.

The cleanest signal for top-charm associated productions at the ILC is $\ell bj + \not{p}_T$ with j being a light quark jet and $\ell = e$ or μ. Generally speaking, the SM irreducible backgrounds for these processes are small due to the odd b-parity of the signal [51]. So far as $e^+e^- \to t\bar{c}$ is concerned, the irreducible SM background arises from $e^+e^- \to W^+W^- \to \bar{c}bl\nu$ and is negligible due to the small size of V_{cb}. The leading SM background then comes from

$$e^+e^- \to q\bar{q}'l\nu, \tag{18}$$

where the light quark jet q or q' may be mis-identified as a b-jet. Such backgrounds, mainly from W pair productions as well as the W bremsstrahlung processes $e^+e^- \to W + 2\,\mathrm{jets}$, can reach 2252 fb in total [52]. Fortunately, these backgrounds can be efficiently suppressed by reconstructing the top-quark mass from the CM energy and the charm jet energy [52], i.e.

$$m_t^{rec} = (s - 2\sqrt{s}E_c)^{1/2}, \tag{19}$$

with $E_c = \frac{\sqrt{s}}{2}(1 - m_t^2/s)$. According to the analysis in [52], the $t\bar{c}$ production with a cross section larger than 1 fb is observable at 95% C.L. for an integrated luminosity of $100\,\mathrm{fb}^{-1}$. From Table 1 one sees that no new physics models can enhance the rate of $e^+e^- \to t\bar{c}$ to the level of 1 fb.

Next we turn to the process $e^+e^- \overset{W^*W^*}{\to} \nu\bar{\nu}t\bar{c}$. The signal is not as distinctive as $e^+e^- \to t\bar{c}$ due to the missing

neutrinos. Its SM reducible background is generated by processes such as $e^+e^- \to W^+W^-\nu_e\bar{\nu}_e$ and $e^+e^- \to t\bar{t}\nu\bar{\nu}_e$. These backgrounds can be suppressed by applying some useful cuts [52]. So far the detailed Monte Carlo simulation for the observability of this process is still lacking. We expect conservatively that the production at the level of several fb may be accessible at the ILC. From Table 1 we see that TC2 model can enhance this production to this level.

Finally, we consider the $\gamma\gamma$ collision. The largest SM background for $\gamma\gamma \to t\bar{c}$ is from $\gamma\gamma \to W^+W^-$, which can reach $\mathcal{O}(10)$ pb. Assuming a fixed CM energy of 500 GeV for $\gamma\gamma$ collisions, a detailed Monte Carlo simulation [39] showed that the background can be neglected at the expense of reducing the signal cross section to 14%. Noting the fact that the cuts used in [39] are not sensitive to the energy of $\gamma\gamma$ collisions, one may infer that this conclusion is approximately valid for a realistic $\gamma\gamma$ collision whose CM energy is not fixed. In fact, this point was also emphasized at the end of Sects. III and IV in [39]. In practice, if we assume conservatively that the signal is reduced to 10% to eliminate backgrounds, we may expect that the production $\gamma\gamma \to t\bar{c}$ as large as 5 fb may be accessible at the ILC at the 3σ level. Compared with the predictions in Table 1, one sees that the TC2 model can enhance the production $\gamma\gamma \to t\bar{c}$ to the observable level at the ILC in a large part of the parameter space.

5 Summary and conclusion

We calculated the top-charm associated productions via e^+e^-, $e^-\gamma$ and $\gamma\gamma$ collisions at linear colliders in the top-color-assisted technicolor model. Then we compared the results with the existing predictions of the SM, the general two-Higgs-doublet model and the minimal supersymmetric model. We observed that the top-color-assisted technicolor model predicts much larger production rates than other models and the largest-rate channel is $\gamma\gamma \to t\bar{c}$, which can exceed 10 fb for a large part of the parameter space. From the analysis of the observability of such productions at the future linear colliders, we conclude that the predictions of the top-color-assisted technicolor model can reach the observable level for a large part of the parameter space while the optimum predictions of other models may lie below the accessible level.

Acknowledgements. This work is supported in part by Young Outstanding Foundation of Academia Sinica, by Chinese Natural Science Foundation under No. 10175017, 10375017 and by the Invitation Program of JSPS under No. L03517.

References

1. For model-independent analyses, see, e.g., C.T. Hill, S.J. Parke, Phys. Rev. D **49**, 4454 (1994); K. Whisnant et al., Phys. Rev. D **56**, 467 (1997); K. Hikasa et al., Phys. Rev. D **58**, 114003 (1998)
2. C.T. Hill, Phys. Lett. B **345**, 483 (1995)
3. K. Lane, E. Eichten, Phys. Lett. B **352**, 382 (1995); K. Lane, Phys. Lett. B **433**, 96 (1998)
4. G. Cvetic, Rev. Mod. Phys. **71**, 513 (1999)
5. E. Malkawi, T. Tait, Phys. Rev. D **54**, 5758 (1996); A. Datta et al., Phys. Rev. D **56**, 3107 (1997); R.J. Oakes et al., Phys. Rev. D **57**, 534 (1998); K. Hikasa, J.M. Yang, B.-L. Young, Phys. Rev. D **60**, 114041 (1999); P. Chiappetta et al., Phys. Rev. D **61**, 115008 (2000);
6. T. Tait, C. P. Yuan, Phys. Rev. D **55**, 7300 (1997); M. Hosch et al., Phys. Rev. D **58**, 034002 (1998); S. Mrenna, C.P. Yuan, Phys. Lett. B **367**, 188 (1996); K.J. Abraham et al., Phys. Lett. B **514**, 72 (2001); Phys. Rev. D **63**, 034011 (2001); F. del Aguila, J.A. Aguilar-Saavedra, R. Miquel, Phys. Rev. Lett. **82**, 1628 (1999)
7. H.J. He, C.P. Yuan, Phys. Rev. Lett. **83**, 28 (1999)
8. G. Burdman, Phys. Rev. Lett. **83**, 2888 (1999)
9. J. Cao, Z. Xiong, J.M. Yang, Phys. Rev. D **67**, 071701 (2003); F. Larios, F. Penunuri, hep-ph/0311056
10. C. Yue et al., Mod. Phys. Lett. A **17**, 2349 (2002); X. Wang et al., Phys. Rev. D **66**, 075009 (2002)
11. For FCNC top-quark decays in TC2 theory, see X.L. Wang et al., Phys. Rev. D **50**, 5781 (1994); C. Yue et al., Phys. Lett. B **508**, 290 (2001); G. Lu, F. Yin, X. Wang, L. Wan, Phys. Rev. D **68**, 015002 (2003)
12. For FCNC top quark decays in the MSSM, see C.S. Li, R.J. Oakes, J.M. Yang, Phys. Rev. D **49**, 293 (1994); G. Couture, C. Hamzaoui, H. Konig, Phys. Rev. D **52**, 1713 (1995); J.L. Lopez, D.V. Nanopoulos, R. Rangarajan, Phys. Rev. D **56**, 3100 (1997); G.M. de Divitiis, R. Petronzio, L. Silvestrini, Nucl. Phys. B **504**, 45 (1997); J.M. Yang, B.-L. Young, X. Zhang, Phys. Rev. D **58**, 055001 (1998); J.M. Yang, C.S. Li, Phys. Rev. D **49**, 3412 (1994); J. Guasch, J. Sola, Nucl. Phys. B **562**, 3 (1999); G. Eilam et al., Phys. Lett. B **510**, 227 (2001); J.J. Liu, C.S. Li, L.L. Yang, L.G. Jin, Phys. Lett. B **599**, 92 (2004)
13. For top-charm associated productions in the MSSM, see J. Cao, Z. Xiong, J.M. Yang, Nucl. Phys. B **651**, 87 (2003); C.S. Li, X. Zhang, S.H. Zhu, Phys. Rev. D **60**, 077702 (1999); J.J. Liu, C.S. Li, L.L. Yang, L.G. Jin, Nucl. Phys. B **705**, 3 (2005)
14. Y. Zeng-Hui et al., Eur. Phys. J. C **16**, 541 (2000)
15. J. Yi et al., Phys. Rev. D **57**, 4343 (1998)
16. C. Yue et al., Phys. Lett. B **525**,301 (2002)
17. C. Yue, G. Liu, Q. Xu, Phys. Lett. B **509**, 294 (2001)
18. C. Yue et al. Phys. Lett. B **496**, 93 (2000)
19. For recent reviews on top quark, see, e.g., C.T. Hill, E. Simmons, hep-ph/0203079; C.-P. Yuan, hep-ph/0203088; E. Simmons, hep-ph/0211335; S. Willenbrock, hep-ph/0211067; D. Chakraborty, J. Konigsberg, D. Rainwater, hep-ph/0303092
20. K. Abe et al., ACFA Linear Collider Working Group, hep-ph/0109166
21. G. Buchalla, G. Burdman, C.T. Hill, D. Kominis, Phys. Rev. D **53**, 5185 (1996)
22. T.P. Cheng, M. Sher, Phys. Rev. D **35**, 3484 (1987); L.J. Hall, S. Weinberg, Phys. Rev. D **48**, 979 (1993)
23. H.E. Haber, G.L. Kane, Phys. Rept. **117**, 75 (1985); J.F. Gunion, H.E. Haber, Nucl. Phys. B **272**, 1 (1986)
24. A. Stange, S. Willenbrock, Phys. Rev. D **48**, 2054 (1993); C.S. Li, J.M. Yang, Y.l. Zhu, H.Y. Zhou, Phys. Rev. D **54**, 4662 (1996); C.S. Li, R.J. Oakes, J.M. Yang, Phys. Rev. D **55**, 1672 (1997); H.Y. Zhou, C.S. Li, Y.P. Kuang, Phys. Rev. D **55**, 4412 (1997)

25. S.J. Brodsky, T. Kinoshita, H. Terazawa, Phys. Rev. D **4**, 1532 (1971); H. Terazawa, Rev. Mod. Phys. **45**, 615 (1973); B.A. Kniehl, Phys. Lett. B **254**, 267 (1991)
26. R. Cahn, S. Dawson, Phys. Lett. B **136**, 196 (1984); M. Chanowitz, M.K. Gaillard, Phys. Lett. B **142**, 85 (1984); G.L. Kane et al., Phys. Lett. B **148**, 367 (1984)
27. I.F. Ginzburg et al., Nucl. Instrum. **219**, 5 (1984); V.I. Telnov, Nucl. Instrum. Meth. **294**, 72 (1990)
28. C.T. Hill, G.G. Ross, Nucl. Phys. B **311**, 253 (1988); Phys. Lett. B **203**, 125 (1988)
29. B. Balaji, Phys. Rev. D **53**, 1699 (1996).
30. H. Pagels, S. Stokar, Phys. Rev. D **20**, 2947 (1979)
31. E. Farhi, L. Susskind, Phys. Rept. **74**, 277 (1981)
32. C.T. Hill, Phys. Lett. B **266**, 419 (1991)
33. R.S. Chivukula, B. Dobrescu, H. Georgi, C.T. Hill, Phys. Rev. D **59**, 075003 (1999)
34. B. Balaji, Phys. Lett. B **393**, 89 (1997)
35. G. Burdman, D. Kominis, Phys. Lett. B **403**, 101 (1997); W. Loinaz, T. Takeuchi, Phys. Rev. D **60**, 015005 (1999)
36. C.T. Hill, X.m. Zhang, Phys. Rev. D **51**, 3563 (1995); C. Yue, Y.P. Kuang, X. Wang, W. Li, Phys. Rev. D **62**, 055005 (2000)
37. Particle Physics Group. Eur. Phys. J. C **15**, 274 (2000); K. Hagiwara et al., Phys. Rev. D **66**, 010001 (2002)
38. A.K. Leibovich, D. Rainwater, Phys. Rev. D **65**, 055012 (2002)
39. K.J. Abraham, K. Whisnant, B.-L. Young, Phys. Lett. B **419**, 381 (1998)
40. D. Atwood, L. Reina, A. Soni, Phys. Rev. D **54**, 3296 (1996); D **55**, 3156 (1997); L. Reina, hep-ph/9712426; M. Sher, hep-ph/9809590; D. Bowser-Chao, K. Cheung, W.Y. Keung, Phys. Rev. D **59**, 115006 (1999)
41. L.J. Hall, R. Rattazzi, U. Sarid, Phys. Rev. D **50**, 7048 (1994); T. Blazek, S. Raby, S. Pokorski, Phys. Rev. D **52**, 4151 (1995); M. Carena, S. Mrenna, C.E.M. Wagner, Phys. Rev. D **60**, 075010 (1999); K.S. Babu, C.F. Kolda, Phys. Lett. B **451**, 77 (1999); Phys. Rev. Lett. **84**, 228 (2000)
42. See, e.g., M. Misiak, S. Pokorski, J. Rosiek, Adv. Ser. Direct. High Energy Phys. **15**, 795 (1998); K. Hikasa, M. Kobayashi, Phys. Rev. D **36**, 724 (1987)
43. S. Bar-Shalom, G. Eilam, A. Soni, J. Wudka, Phys. Rev. Lett. **79**, 1217 (1997); Phys. Rev. D **57**, 2957 (1998)
44. C.S. Huang, X.H. Wu, S.H. Zhu, Phys. Lett. B **452**, 143 (1999)
45. D. Atwood, L. Reina, A. Soni, Phys. Rev. D **53**, 1199 (1996)
46. G. Eilam, J.L. Hewett, A. Soni, Phys. Rev. D **44**, 1473 (1991); B. Mele, S. Petrarca, A. Soddu, Phys. Lett. B **435**, 401 (1998)
47. D. Atwood, L. Reina, A. Soni, Phys. Rev. D **55**, 3156 (1997); R.A. Diaz, R. Martinez, J.A. Rodriguez, hep-ph/0103307.
48. J. Guasch, J. Sola, hep-ph/9909503; S. Bejar, J. Guasch, J. Sola, Nucl. Phys. B **600**, 21 (2001)
49. F. Abe et al., CDF Collaboration, Phys. Rev. Lett. **80**, 2525 (1998); J.A. Aguilar-Saavedra, G.C. Branco, Phys. Lett. B **495**, 347 (2000);
50. R. Frey et al., FERMILAB-CONF-97-085 (1997); hep-ph/9704243
51. S. Bar-Sharlom, J. Wudka, Phys. Rev. Lett. **86**, 3722 (2001)
52. T. Han, J.L. Hewett, Phys. Rev. D **60**, 074015 (1999); S. Bar-Shalom, J. Wudka, Phys. Rev. D **60**, 094016 (1999); J.A. Aguilar-Saavedra, Phys. Lett. B **502**, 115 (2001); J.A. Aguilar-Saavedra, T. Riemann, hep-ph/0102197